Precursor-Mediated Molecular Chemisorption and Thermal Desorption: The Interrelationships among Energetics, Kinetics, and Adsorbate Lattice Structure

Eric S. Hood, Brian H. Toby, and W. H. Weinberg

Division of Chemistry and Chemical Engineering, California Institute of Technology, Pasadena, California 91125

(Received 24 June 1985)

Precursor-mediated molecular chemisorption and thermal desorption are examined by means of a lattice-gas model using a combination of time-dependent Monte Carlo simulations and deterministic rate equations. Lateral interactions between coadsorbates are assumed to be both pairwise additive and limited in range to nearest and next-nearest neighbors. The interrelationships among kinetics, energetics, and adsorbate overlayer structures are analyzed in detail. The method is applied to the interaction of molecular nitrogen with the Ru(001) surface.

PACS numbers: 68.40.+e, 68.20.+t, 82.65.Dp

Although the concept of a physically adsorbed, "mobile precursor" state is not new,[1] much recent experimental effort has been directed toward the understanding of the phenomenon of precursor-mediated chemisorption.[2] Likewise, the influence of mobile precursor states on the kinetics of molecular chemisorption and desorption has been examined theoretically both by a reaction kinetics approach[3] and by statistical modeling.[4] In this Letter we introduce a theoretical modeling scheme for the study of precursor-mediated molecular chemisorption and thermal desorption, incorporating a combination of Monte Carlo simulations and deterministic rate equations with a stochastic formulation. The novelty of our approach lies in the simultaneous treatment of the various, competing elementary processes (physical adsorption, migration, chemisorption, and desorption) within a single, integrated model. In contrast to previous theoretical treatments, the microscopic detail inherent in our approach allows direct examination of the interrelationships among kinetics, energetics, and the formation and evolution of structure within the adsorbate overlayer. Numerical simulations provide a clear demonstration of the profound effects of island formation and growth.

Molecular chemisorption from a mobile precursor state is examined by use of a lattice gas model and time-dependent Monte Carlo (TDMC) simulations.[5] Molecules are placed sequentially on randomly chosen surface sites to simulate trapping from the gas phase into a physically adsorbed precursor state. Each precursor molecule migrates across the surface in single jumps to nearest-neighbor (nn) sites. This mobile intermediate state is occupied until either desorption or chemisorption occurs. The binding energy of the precursor is a function of the local molecular environment because of lateral interactions with previously chemisorbed molecules [assumed to be pairwise additive and limited in range to nn and nnn (next-nearest neighbor) adsorbates]. The binding energy of a molecule physically absorbed over an unoccupied lattice site (the intrinsic precursor state) is given by

$$\epsilon_p = \epsilon_0 - \sum_j n_j \epsilon_r + \sum_k n_k \epsilon_a, \tag{1}$$

where ϵ_0 is the binding energy of an isolated precursor to the surface, and ϵ_r and ϵ_a are the repulsive and attractive energies of interaction between the precursor and a neighboring *chemisorbed* molecule. The sums in Eq. (1) are performed over nn (j) and nnn (k) lattice sites, and n_j and n_k are occupation numbers. The binding energy (ϵ_n) of a molecule physically absorbed over a lattice site occupied by a chemisorbed molecule (the extrinsic precursor state) is assumed to have a constant value, 85% of ϵ_0.[6]

Each precursor molecule is temporarily confined to a particular lattice site by a periodic potential parallel to the surface, represented by adjacent, intersecting harmonic wells. The relative depths of neighboring potential-energy minima are computed according to Eq. (1). The activation barrier to precursor migration is given by the energy at the intersection point between adjacent harmonic potentials:

$$\epsilon_m = \epsilon_m^0 + \Delta\epsilon_p(i,j)/2 + [\Delta\epsilon_p(i,j)]^2/16\epsilon_m^0, \tag{2}$$

where ϵ_m^0 is the activation barrier to migration of an isolated intrinsic precursor molecule, and $\Delta\epsilon_p(i,j)$ is the difference in precursor binding energies between the ith and jth sites [$\Delta\epsilon_p(i,j) \equiv \epsilon_p(j) - \epsilon_p(i)$]. The probability for precursor migration from the ith to the neighboring jth lattice site is given by $P_m(i,j) = N\exp(-\epsilon_m/k_BT)$, where the constant N ensures unitarity. The probability for precursor desorption is given by $P_d = N\chi\exp(-\epsilon_p/k_BT)$, where the dynamical factor χ is the ratio between desorption and migration prefactors. The probability of molecular chemisorption is

$$P_c = [N\chi S_0 \exp(-\epsilon_0/k_BT)]/(1-S_0),$$

where S_0 is the initial (zero coverage) adsorption coef-

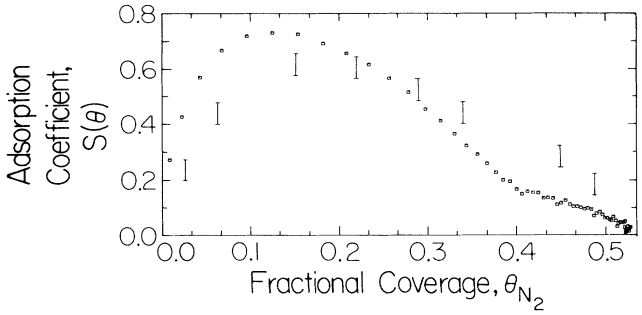

FIG. 1. Adsorption coefficient as a function of coverage for N_2 on Ru(001) at 77 K. Vertical bars represent experimental results (Ref. 9), while squares represent averages over eight TDMC simulations.

ficient. The relative probabilities of precursor desorption, migration to an adjacent site, or chemisorption are all functions of the local molecular environment. Maps displaying the locations of chemisorbed molecules can be constructed which detail the growth of adsorbate lattice structure as a function of coverage.

Thermal-desorption spectra (TDS) have been computed by use of a combination of deterministic rate equations with a Monte Carlo formalism.[5] Even though a single binding site and geometry are assumed, chemisorbed molecules can populate a number of energetically distinct binding states, characterized by different activation barriers to desorption $[\epsilon_b(i)]$ which are determined by the numbers and magnitudes of lateral interactions between the chemisorbed molecules, i.e.,

$$\epsilon_b(i) = \epsilon_b^0 - \sum_j n_j \tilde{\epsilon}_r + \sum_k n_k \tilde{\epsilon}_a. \quad (3)$$

In Eq. (3) ϵ_b^0 is the binding energy of an isolated chemisorbed molecule, and $\tilde{\epsilon}_r$ and $\tilde{\epsilon}_a$ are the repulsive and attractive energies of interaction between neighboring chemisorbed molecules. The rate of desorption from each chemisorption state is computed with use of a modified first-order Polanyi-Wigner equation with a coverage-dependent preexponential factor,[7]

$$d\sigma_i/dt = -\nu(\theta)\sigma_i \exp[-\epsilon_b(i)/k_B T], \quad (4)$$

with $\nu(\theta) \equiv \nu_0 \exp(\alpha\theta)$.[8] In Eq. (4) σ_i is the occupation number of the ith chemisorption state, and θ is the fractional coverage of chemisorbed molecules. The system of coupled differential equations describing desorption from all chemisorption states is solved numerically. During each computational cycle ($\Delta T \lesssim 0.5$ K), the appropriate number of molecules is selected from each chemisorption state according to Eq. (4) and removed from randomly chosen lattice sites to avoid the introduction of artificial correlation effects. The calculation is repeated until all molecules have desorbed.

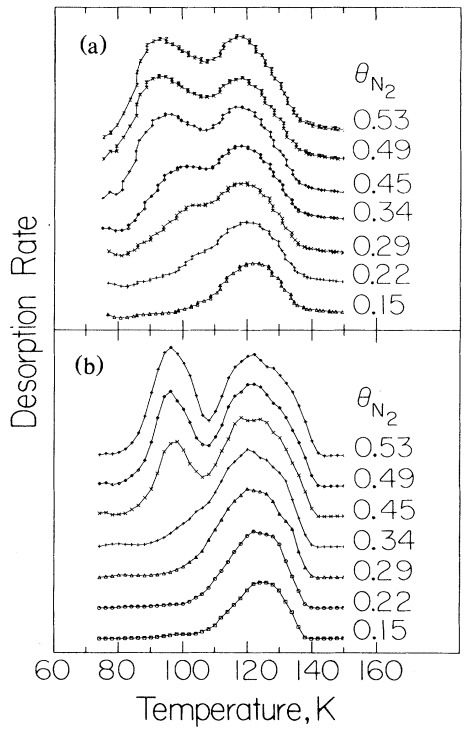

FIG. 2. Thermal-desorption spectra for N_2 on Ru(001) at various adsorbate coverages: (a) experimental results (Ref. 9), and (b) TDMC simulation and thermal-desorption modeling.

The interaction of N_2 with the Ru(001) surface has been examined by this methodology. The results of TDMC simulations are in good agreement with the experimentally measured adsorption coefficient[9,10] (cf. Fig. 1). Experimentally measured TDS are shown in Fig. 2(a). Although two peaks are observed at adsorbate coverages above 0.25, electron energy-loss spectra indicate that chemisorption of N_2 occurs only at atop sites.[10] Figure 2(b) shows TDS computed with the assumption of *a single binding geometry at atop sites.* Quantitative agreement between calculated and experimental thermal-desorption spectra is obtained for all adsorbate coverages.

TDMC simulations of N_2 adsorption on Ru(001) have been performed for a surface temperature of 77 K on a lattice composed of 9216 Ru atoms. Maps indicating the locations of chemisorbed N_2 molecules chart the growth of adsorbate lattice structure as a function of coverage (cf. Fig. 3). Because of the hexagonal geometry of Ru(001) and the nature and magnitude of adsorbate interactions, the energetically favored overlayer structure (as indicated by a well-developed LEED pattern[9] at 95 K) possesses $(\sqrt{3}\times\sqrt{3})R30°$ symmetry. However, three independent, degenerate adsorbate phases can exist on this hexagonal surface which are distinguishable by 120° rotations about a

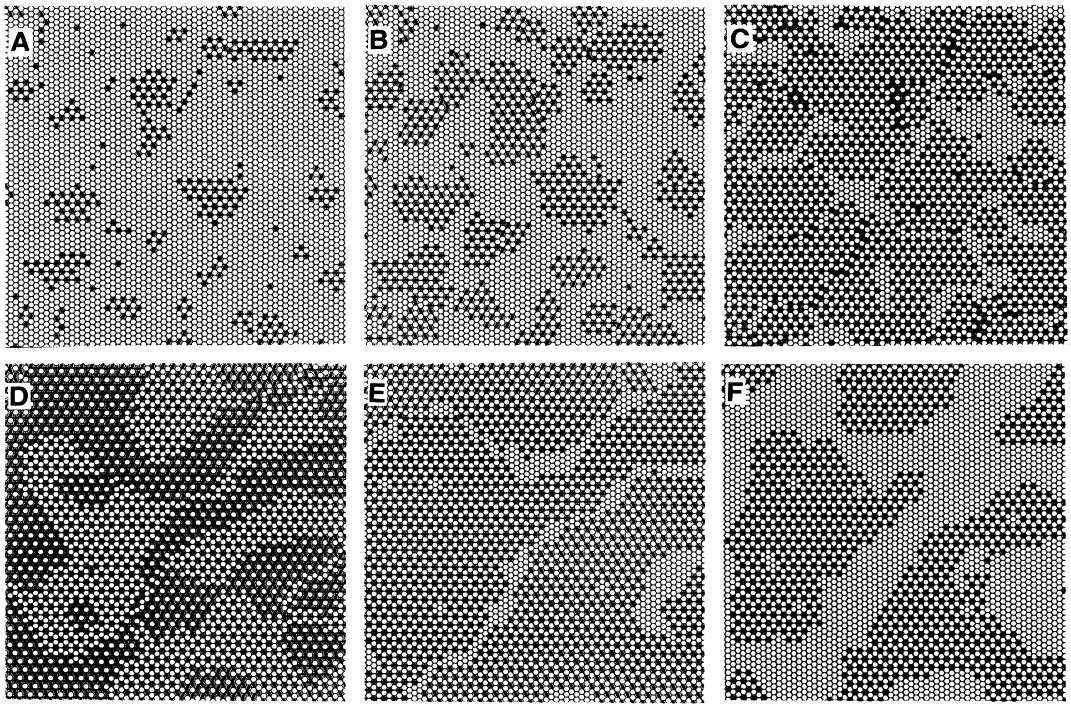

FIG. 3. Maps displaying the locations of N_2 chemisorbed on sections of the Ru(001) surface generated by (a)–(d) TDMC simulations of adsorption, and (e),(f) thermal-desorption modeling. Open circles represent surface Ru atoms, while dots represent N_2 chemisorbed atop Ru surface atoms. The solid lines represent the three degenerate phases characterizing this system. The fractional N_2 coverages are (a) 0.06, (b) 0.15, (c) 0.29, (d) 0.53, (e) 0.29, and (f) 0.15.

threefold axis centered within the triangle formed by three adjacent Ru atoms. Distinct adsorbate domains can be observed on a surface where two or more of these phases coexist.

An examination of both $S(\theta)$ and maps of the chemisorbed overlayer allows a detailed description of the adsorption process. Chemisorption at 77 K occurs in four distinct stages: (I) island nucleation, (II) growth of isolated island domains, (III) simulataneous growth of island domains and antiphase-domain boundaries, and (IV) growth of antiphase domains. The chemisorption of isolated molecules, acting as nucleation centers for the growth of numerous, small island domains, characterizes stage I [cf. Fig. 3(a)]. Cooperative behavior dominates stage II as $S(\theta)$ undergoes a threefold increase. Increasing order is observed in the chemisorbed overlayer as the edges of island domains serve as the most probable sites for chemisorption [cf. Fig. 3(b)]. The growth of isolated island domains continues up to a fractional coverage of approximately 0.22. "Crowding" between neighboring islands signals the onset of growth stage III [cf. Fig. 3(c)]. Adjacent domains of the same phase coalesce to form larger islands, while adjacent domains of differing phase develop grain boundaries. During stage III, $S(\theta)$ suffers a fivefold decrease as appreciable chemisorption occurs at grain boundaries in addition to the more energetically favorable island domains. The onset of stage IV is accompanied by a change in the slope of $S(\theta)$ at 0.4 monolayer (cf. Fig. 1). At adsorbate coverages above 0.4, chemisorption occurs in regions of antiphase domains. Saturation coverage occurs at approximately 0.55 because of a steady-state balance between the rate of precursor-mediated adsorption and the rate of desorption from the chemisorbed states [cf. Fig. 3(d)].

The influence of lateral interactions between coadsorbates on the kinetics and mechanism of molecular desorption can be evaluated by an examination of both the adsorbate lattice maps and the coverage-dependent TDS. For coverages below 0.25, the TDS consist of a single peak at a surface temperature of approximately 125 K. This peak is associated with desorption from the perimeters of isolated islands. The N_2 chemisorbed within isolated islands experience attractive lateral interactions which increase the activation barrier to desorption above that experienced by an isolated adsorbate. At adsorbate coverages above 0.3, a second peak at a surface temperature below 100 K appears in the TDS. This peak is associated with desorption from antiphase domains. Molecular N_2 chemisorbed within these antiphase domains experience

TABLE I. Kinetic and energetic parameters characterizing the interaction of molecular nitrogen with Ru(001) with energy in units of kcal/mole.

ϵ_0: Intrinsic precursor binding energy	1.6
ϵ_n: Extrinsic precursor binding energy	1.4
ϵ_b^0: Chemisorption state binding energy	5.8
ϵ_m^0: Precursor state migration barrier	0.3
$\epsilon_a, \tilde{\epsilon}_a$: Attractive next-nearest-neighbor interaction energy	0.45
$\epsilon_r, \tilde{\epsilon}_r$: Repulsive nearest-neighbor interaction energy	0.25
χ: Ratio of precursor preexponential factors of desorption to migration	500–1000
ν_0: Desorption preexponential factor (low coverage limit)	10^{12} s^{-1}
α: Desorption preexponential coverage dependence	17

repulsive lateral interactions which decrease the activation barrier to desorption. At saturation coverage, the number of molecules desorbing from antiphase domains and the number desorbing from isolated-island perimeters are nearly equal, as are the intensities of the two thermal desorption peaks. The value of this type of numerical simulation is clearly evident: By the relating of the adsorbate structure to kinetic measurements, the two peaks appearing in the "high"-coverage ($\theta \gtrsim 0.3$) TDS are shown to result solely from lateral interactions between molecules chemisorbed only at atop sites [cf. Figs. 3(d)–3(f)].

Numerical values of the parameters characterizing the system N_2 on Ru(001) (Table I) are obtained by minimization of the differences between the calculated and experimental coverage-dependent adsorption coefficients and TDS. Although precursor-state–chemisorption-state and chemisorption-state–chemisorption-state lateral interaction energies are treated as separate parameters, adsorption and desorption simulations yield nearly identical values for both. *This similarity in lateral interaction energetics is due primarily to the weak binding energy of chemisorbed molecular nitrogen on this surface.*

Examination of the maps of adsorbate positions as a function of coverage reveals obvious differences between the mechanisms of precursor-mediated molecular chemisorption and thermal desorption from the chemisorbed state. The absorption mechanism is dominated by kinetic trapping which results in the formation of numerous, small island domains [cf. Fig. 3(a)–3(d)]. Thermal desorption is dominated by relaxation (annealing), as evidenced by the formation of fewer, but much larger, island domains [cf. Figs. 3(e) and 3(f)]. The ability to disclose in microscopic detail the interrelationships among energetics, kinetics, and adsorbate overlayer structures demonstrates the value of this integrated approach to molecular chemisorption and thermal-desorption simulations.

This work was supported by the National Science Foundation under Grant No. CHE-8206487. One of us (E.S.H.) acknowledges receipt of a Bantrell Postdoctoral Fellowship.

[1]J. B. Taylor and I. Langmuir, Phys. Rev. **44**, 423 (1933).

[2]P. Alnot and D. A. King, Surf. Sci. **126**, 359 (1983); H. Pfnür and D. Menzel, J. Chem. Phys. **79**, 2400 (1983); M. Grunze, J. Fuhler, M. Neumann, C. Brundle, D. Auerbach, and J. Behm, Surf. Sci. **139**, 109 (1984); S. Tang, M. Lee, J. Beckerle, M. Hines, and S. Ceyer, J. Chem. Phys. **82**, 2826 (1985); M. Shayegan, E. D. Williams, R. E. Glover, and R. L. Park, Surf. Sci. **154**, L239 (1985).

[3]D. A. King and M. Wells, Proc. Roy. Soc. London, Ser. A **339**, 245 (1974); R. Gorte and L. Schmidt, Surf. Sci. **76**, 559 (1978); D. L. Freeman and J. D. Doll, J. Chem. Phys. **78**, 6002 (1983), and **79**, 2343 (1983).

[4]P. Kisliuk, J. Phys. Chem. Solids **3**, 95 (1957), and **5**, 78 (1958); D. A. King, Surf. Sci. **64**, 43 (1977); A. Cassuto and D. A. King, Surf. Sci. **102**, 388 (1981); J. E. Adams and J. D. Doll, Surf. Sci. **103**, 472 (1981), and **111**, 492 (1981).

[5]E. S. Hood, B. H. Toby, and W. H. Weinberg, unpublished.

[6]K. Christmann and J. Demuth, Surf. Sci. **120**, 291 (1982).

[7]P. Redhead, Vacuum **12**, 203 (1962); D. Adams, Surf. Sci. **42**, 12 (1974).

[8]A number of different functional forms for $\nu(\theta)$ have been tested, including the form presente by P. Feulner and D. Menzel, Phys. Rev. B **25**, 4295 (1982), and D. Menzel, H. Pfnür, and P. Feulner, Surf. Sci. **126**, 374 (1983). TDS computed with use of the exponential coverage dependence were in closest agreement with experimental results.

[9]Feulner and Menzel, Ref. 8; Menzel, Pfnür, and Feulner, Ref. 8.

[10]A. Anton, N. Avery, B. Toby, and W. H. Weinberg, J. Electron Spectrosc. Relat. Phenom. **29**, 181 (1983).